ELSEVIER

Journal of Nuclear Materials 245 (1997) 238–247

journal of nuclear materials

A review of kinetic data on the rate of U_3O_7 formation on UO_2

R.J. McEachern *

Research Chemistry Branch, AECL, Whiteshell Laboratories, Pinawa, Manitoba, Canada ROE 1LO

Received 6 August 1996; accepted 20 November 1996

Abstract

Kinetic data on the rate of U_3O_7 formation on UO_2 have been critically reviewed. Oxidation of UO_2 powders displays diffusion-controlled (parabolic) kinetics, whereas sintered UO_2 pellets display approximately linear kinetics, presumably because the rate of oxidation in the latter is limited by a combination of cracking, intragranular and grain-boundary oxidation. The activation energy for the formation of U_3O_7 on UO_2 is estimated to be 96 kJ mol^{-1} for powders and 99 kJ mol^{-1} for sintered pellets. Analysis of kinetic data suggests that the formation of U_4O_9/U_3O_7 may have a significant impact on weight-gain oxidation experiments with used nuclear fuel and should thus be considered when estimating the rate of U_3O_8 formation.

1. Introduction

The two-stage oxidation reaction of UO_2

$$UO_2 \rightarrow U_3O_7 \rightarrow U_3O_8 \quad (1)$$

has been studied extensively for over 40 years [1–5]. Much of the more recent work has been concerned with the significance of air oxidation to the dry storage and ultimate disposal of used nuclear fuel [6–10]. The formation of U_3O_8 has been studied extensively because there is a 36% volume increase upon oxidation of UO_2 to U_3O_8. Thus the formation of U_3O_8 in a previously defected fuel element can lead to splitting of the sheath [8,11–13], which can complicate subsequent handling and disposal of the fuel.

The kinetics of U_3O_7 formation have not been analyzed as rigorously as they have for the subsequent reaction to form U_3O_8. In part this is because the formation of the intermediate U_3O_7 has little impact on fuel integrity, but also because it is often difficult to deconvolute the first stage of the oxidation reaction from the second, especially for sintered pellets. However, any serious effort to understand UO_2 oxidation kinetics and thus predict accurately the behaviour of used nuclear fuel under dry air storage conditions, cannot ignore U_3O_7 formation. Published data on the rate of formation of U_3O_7 have therefore been critically reviewed and the results are presented herein.

2. Mechanism for the formation of U_3O_7

A more accurate description than Eq. (1) for the first stage of UO_2 oxidation is

$$UO_2 \rightarrow U_3O_7/U_4O_{9+y} \quad (2)$$

because the structure of the product depends on the nature of the fuel and the oxidation conditions. Low-temperature oxidation of unirradiated fuel, or UO_2 doped with low concentrations of impurities results in the formation of 'U_3O_7'. There remains considerable confusion on the nature of the U_3O_7 thus formed. Several tetragonal phases with composition near $UO_{2.33}$ have been reported depending on the nature of sample preparation. In contrast, cubic 'U_4O_{9+y}' is the product of oxidation of spent light water reactor (LWR) fuel or highly doped UO_2 [14]. In the case of used LWR fuel oxidation, the U_4O_9 thus formed has the stoichiometry $\sim UO_{2.4}$ and structure similar to that of γ-U_4O_9 [14].

The structure of U_3O_7 is related to that of U_4O_9 in the sense that they both incorporate excess oxygen anions interstitially in the UO_2 (fluorite-type) structure [15–17]. Moreover, parabolic kinetics are observed for both the

* Tel: +1-204 753 2311; fax: +1-204 753 2455.

PII S0022-3115(96)00733-7

formation of U_3O_7 and U_4O_9. It thus seems reasonable to assume that the diffusion-controlled mechanism for the intragranular oxidation to form U_3O_7 is essentially the same as that of U_4O_9. Therefore, the term 'U_4O_9/U_3O_7' or the unqualified term 'U_3O_7' is used herein to refer to the product of the first stage of air oxidation of UO_2, except in the case of used LWR fuel, in which case the oxidation product is clearly a cubic substance approximating U_4O_9 [18]. We note that other fluorite-derivative phases such as $UO_{2.3}$ and U_8O_{19} have also been occasionally reported as oxidation products on UO_2 [19,20]; for the present discussion, these too are described by the term U_4O_9/U_3O_7.

The oxidation behaviour of UO_2 varies depending on the form of the material, that is, whether it is a powder or pellet and whether or not it has been irradiated. Each type of fuel is thus examined separately in the following sections.

2.1. UO_2 powders

There is general agreement that the formation of U_3O_7 on UO_2 powders proceeds via parabolic reaction kinetics, which indicates that the reaction is diffusion controlled [1,3,5,21–24]. Two mechanisms are consistent with the generally accepted diffusion-controlled kinetics for the oxidation of UO_2 powders. For illustration, consider oxidation of UO_2 spheres of radius, r. In the first (the 'concentration gradient') mechanism it is assumed that there is adequate solubility of oxygen in UO_2 so that a solid solution, UO_{2+x}, is formed along a concentration gradient inside the particle. The material is then converted to U_3O_7 when enough oxygen has been incorporated into the lattice so that its composition is in the range $UO_{2.25}$ to $UO_{2.34}$. According to the concentration-gradient mechanism, the fraction of the material (f) oxidized at time (t) is given by [1,25]

$$f = 1 - \frac{6}{\pi^2}\sum_{n=1}^{\infty}\left(\frac{1}{n^2}\right)\exp\left(-\frac{\pi^2 n^2 Dt}{r^2}\right), \tag{3}$$

where D is the diffusion coefficient of oxygen in UO_2 and r is the radius of each spherical particle.

A second (the 'discrete-layer') mechanism has also been used to describe the formation of U_3O_7 on UO_2. According to this model, oxidation proceeds by the formation of a discrete layer of U_3O_7 on the sample surface. The oxide layer grows thicker with time and the rate of reaction is limited by the rate of diffusion of oxygen through the U_3O_7 layer. The thickness, τ, of the product layer is given by [4,26–28]

$$\tau = ra\left[1 - (1-f)^{1/3}\right] = \sqrt{kt}, \tag{4}$$

where r is the radius of the initial UO_2 particle, f is the degree of bulk oxidation, k is the diffusion-controlled rate constant and a is the ratio of the molar volume of the product to that of the starting material (~ 0.99 for the formation of U_3O_7 on UO_2).

It has long been recognized that the two different diffusion-controlled mechanisms yield nearly identical reaction curves [1,4,10,22]. Two different schools of thought thus evolved, and various arguments were presented to support one or the other view. The bulk of the evidence now supports the discrete layer mechanism. The detection of U_3O_7 on the surface of sintered pellets or powder that has a large particle size [3,4] suggests that earlier workers [1,5,22,29] did not observe the tetragonal phase in the early stages of oxidation because the deviations from cubic symmetry are only slight and readily obscured by line broadening associated with the formation of a thin highly oxidized layer on the surface of their very fine powders [3]. Moreover, the formation of a thin surface layer of highly oxidized material results in high weight gains at an early stage of the reaction for fine powders.

Recent work using backscattered-electron scanning electron microscopy (SEM) imaging [9,30] has allowed the direct observation of the formation of U_4O_{9+y} on the surface of individual UO_2 grains in sintered fuel pellets. Thomas and Einziger [9] and Thomas et al. [14] have thus shown clearly that dry air oxidation of used LWR fuel at 175 to 195°C proceeds by the formation of a discrete layer of U_4O_{9+y}. Such observations do not prove conclusively that oxygenic diffusion through the product oxide layer is the rate-limiting step, since it is conceivable that the formation of U_4O_9/U_3O_7 may be preceded by the rate-determining formation of a sub-stoichiometric oxide:

$$UO_2 \rightarrow UO_{2+x}. \tag{5}$$

However, the maximum value of x under dry air storage conditions is probably less than 0.01 [4,31] so it seems reasonable to conclude that oxygen diffusion through the U_4O_9/U_3O_7 product layer is the rate-determining step in the first stage of UO_2 oxidation.

2.2. Unirradiated UO_2 pellets

The oxidation mechanism for sintered pellets is less clear than it is for UO_2 powders. Several investigators have reported that linear oxidation kinetics are observed on the surface of sintered UO_2 pellets [32–34] whereas others have reported that parabolic kinetics apply to fuel pellets, at least in the early stages of U_3O_7 formation [4].

It seems likely that the formation of U_3O_7 on the surface of sintered pellets proceeds initially by parabolic kinetics, but changes to a linear process at an early stage of the reaction. Blackburn et al. [4] reported that parabolic kinetics were observed up to 65% reaction for a powdered UO_2 sample. In contrast, Eq. (4) was only followed for $\sim 1\%$ of the reaction for sintered pellets. The U_3O_7 layer is initially homogeneous on the surface of sintered pellets but then takes on the form of a convoluted 'oxidation front' because intragranular oxidation proceeds more slowly than oxidation along the grain boundaries [32]. Preferential diffusion of oxygen along grain boundaries complicates the oxidation kinetics and may contribute to

the experimentally observed linear reaction kinetics. Crack formation also plays a role in U_3O_7-formation kinetics [33]. The small reduction in molar volume associated with the first stage of oxidation leads to cracking (primarily intragranular and sometimes transgranular), which may dominate the kinetic expression by controlling the rate of ingress of oxygen to the sample [9,33] and lead to linear oxidation kinetics. The degree of intergranular oxidation is usually much less in unirradiated than irradiated fuel (see Section 2.3). Thomas et al. [35] have reported that unirradiated LWR fuel does not display significant grain-boundary oxidation, whereas it is normally observed in unirradiated CANDU [1] fuel specimens, but to varying degrees [36].

2.3. Used fuel

The backscattered-electron SEM technique has recently been used to directly observe the formation of U_4O_9 on used LWR fuel. Such experiments revealed [9,14,18] that the initial stage of dry air oxidation at 175 to 195°C is rapid grain-boundary oxidation. The U_4O_9 product is formed, initially at the intersection of two or more grain boundaries and then spreading along the grain boundaries, so that a contiguous network of U_4O_9 forms as a discrete layer around each grain. Oxidation then proceeds into each grain simultaneously [18].

The nature of the oxidation process suggested to Woodley et al. [37,38] that air oxidation of used LWR fuel can be considered equivalent to oxidation of a UO_2 powder with particle size equal to the grain size of the used fuel. Their data displayed an induction time, during which oxygen permeated the grain boundaries, and then a stage in which the kinetic data could be fitted to an equation similar to Eq. (4). They recognized that the use of Eq. (4) to model their data included a number of assumptions, including a thin product layer and spherical grains. Nonetheless, Woodley et al. [37,38] were able to model their oxidation data successfully.

Oxygenic diffusion along grain boundaries in used LWR fuel is very rapid, presumably because of microscopic fission-gas bubbles and radiation-induced defects present along the grain boundaries [35]. Rapid diffusion of oxygen along grain boundaries causes oxidation of used LWR fuel to proceed simultaneously throughout much or all of the fuel fragment [9,39]. The low-temperature oxidation behaviour of used CANDU fuel is intermediate between that of used LWR fuel and unirradiated UO_2. Grain boundary oxidation in used CANDU fuel typically varies from one part of the sample to another, so that some regions display a distinct oxidation front, while other regions display simultaneous oxidation of individual UO_2 grains [6]. The oxidation behaviour of used CANDU fuel is presumably different from that of used LWR fuel because the former has fewer fission-gas bubbles along the grain boundaries, or because of different in-reactor operating conditions.

It should be noted that the preceding discussion is somewhat oversimplified. Used nuclear fuel is not a homogeneous material and there has been ample evidence to suggest that certain regions of some used LWR fuel samples do not display extremely rapid oxygen diffusion along the grain boundaries. Thus some samples display regions of inhomogeneous oxidation and the existence of oxidation fronts [40]. Sample inhomogeneity and transgranular crack formation [9] suggest that any rigorous model for the oxidation of used fuel will be complex.

3. Kinetic data

Kinetic data for the two types of models (parabolic and linear) for U_3O_7 formation are presented separately. Some exceptions have been noted, but in general the parabolic kinetic data applies to UO_2 powder or used LWR fuel, whereas the linear kinetics apply to unirradiated sintered UO_2 pellets (see Section 2).

3.1. Parabolic kinetic data

It has been recognized for many years that the low-temperature oxidation of UO_2 powders is a diffusion-controlled process. The parabolic kinetic data are thus typically fitted to an equation of the form

$$\tau = \sqrt{kt}\,, \tag{6}$$

where τ is the thickness of the U_3O_7 layer on the surface of individual UO_2 particles and t is the time in seconds. Values of the parabolic rate constant (k) have been tabulated herein. In addition, the results published by Anderson et al. [5] and Aronson et al. [1] have been converted from the concentration-gradient model that they used, to the discrete-layer model, so that these data may be included in the present compilation.

Many of the data presented herein were reported some time ago, so that SI units were not in common usage. For clarity, the data are presented and discussed in the following sections in their original units. However, the results have been converted to SI for the compilation given in Table 1.

3.1.1. The data of Anderson et al.

Anderson et al. [5] studied UO_2 oxidation by measuring the pressure drop associated with U_3O_7 formation. Data were fitted to the expression

$$C = K\sqrt{t} + A \tag{7}$$

where C is the measured consumption of oxygen gas in

[1] Canada Deuterium Uranium, registered trademark of AECL.

Table 1
Parabolic rate constants for the first stage of UO_2 oxidation

Investigator	Sample	Method	Temp. (°C)	k (m^2 s^{-1})
Blackburn et al. (1958)	UO_2 pellets	grav.	125	9.34×10^{-21}
			138	2.79×10^{-20}
			160	9.19×10^{-20}
			189	3.29×10^{-19}
			190	3.88×10^{-19}
			200	6.82×10^{-19}
			210	1.13×10^{-18}
			219	2.94×10^{-18}
			220	2.01×10^{-18}
			231	3.60×10^{-18}
			251	8.02×10^{-18}
			270	1.40×10^{-17}
			280	2.04×10^{-17}
	UO_2 powder	grav.	256	7.88×10^{-18}
Einziger et al. (1992)	spent LWR fuel	SEM	175	1.11×10^{-19}
			195	3.50×10^{-19}
Woodley et al. (1988, 1989)	spent LWR fuel	grav.	175	2.4×10^{-18}
			176	6.1×10^{-19}
			200	7.5×10^{-18}
			200	4.9×10^{-18}
			225	2.6×10^{-17}
			225	6.1×10^{-18}
			225	2.3×10^{-17}
			225	1.7×10^{-17}
Anderson et al. (1955)	UO_2 powder	ΔP	164.5	2.73×10^{-19}
			131	2.54×10^{-20}
Walker (1965)	UO_2 powder	grav.	143	2.02×10^{-20}
			152	4.14×10^{-20}
			161	8.23×10^{-20}
			164	1.03×10^{-19}
			174	2.11×10^{-19}
			182	3.67×10^{-19}
			190	6.27×10^{-19}
			200	1.19×10^{-18}
			211	2.34×10^{-18}

cm^3 (STP [2]) g^{-1}, t is the time in minutes and K and A are empirically determined rate constants. The rate constant, K, has units of cm^3 (STP) $min^{-1/2}$ g^{-1}. It can be shown that the rate constant, K, of Eq. (7) is related to the thickness, τ, of the U_3O_7 layer on the surface of individual UO_2 particles by the expression

$$\tau = \frac{2rKPM_{UO_2}}{1000\sqrt{60}\,RT}\sqrt{t}, \tag{8}$$

where

r = particle radii (m).
P = 1.00 atm.
M_{UO2} = molecular weight of UO_2 = 270.03 g mol^{-1}.
R = 0.08206 l atm mol^{-1} K^{-1}.
T = 273.15 K.
t = time in seconds.

Comparison of Eqs. (6) and (8) shows that the parabolic rate constant, k (m^2 s^{-1}) is given by the expression

$$k = \left(\frac{2rKPM_{UO_2}}{1000RT\sqrt{60}}\right)^2. \tag{9}$$

Anderson et al. [5] reported UO_2 oxidation kinetic data for a variety of pressures between 0.020 and 490 Torr (2.67 and 65 300 Pa). Their data suggest that there is a significant influence of oxygen pressure on the rate of oxidation, so only kinetic data for experiments performed with an oxygen pressure of 120 Torr have been calculated as an

[2] Standard Temperature (273.15 K) and Pressure (101.325 kPa)

approximation to oxidation in air. Values of the rate constant, k, calculated by Eq. (9) for a fine powder ($r = 2.05 \times 10^{-7}$ m) have been included in Table 1.

3.1.2. The data of Aronson et al.

One of the seminal papers on UO_2 oxidation was published nearly 40 years ago by Aronson et al. [1], who oxidized finely powdered UO_2 in dry air in the range 159 to 350°C. Unfortunately, their results were published before there was widespread acceptance of the discrete-layer mechanism for U_3O_7 formation [4]. Thus Aronson et al. [1] fitted the parabolic portion of their weight-gain curves to Eq. (3) for U_3O_7 formation along a concentration gradient.

Kinetic data were reported in terms of D, the oxygen diffusion coefficient and r, the radius of the initial UO_2 particle. The kinetic data reported by Aronson et al. [1] have been converted to rate constants by using Eq. (3) to calculate the time required for 50% reaction (i.e., $f = 0.5$). The rate constant, κ, was then calculated by using these values of f and t in equation

$$1 - [1 - f]^{1/3} = (\kappa t)^{1/2}, \tag{10}$$

where f is the fraction of sample oxidized (assuming that U_3O_7 is the end product for the first stage of oxidation), t is the time in seconds and κ is an empirically determined rate constant.

Eq. (10) is similar to Eq. (6), which describes the product-layer thickness (τ) as a function of time for a diffusion-controlled reaction on the surface of a particle. If the starting material consists of spherical particles, Eq. (6) can be expanded [4,28] to Eq. (4). Comparison of Eqs. (4) and (10) gives the relationship between the constants k and κ:

$$k = (ra)^2 \kappa. \tag{11}$$

Eq. (11) was then used to convert the kinetic data of Aronson et al. [1] into values of the discrete-layer mechanism rate constant, k. The results of the converted kinetic data are presented in Table 2.

3.1.3. The data of Blackburn et al.

Blackburn et al. [4] were among the first to examine the kinetics of U_3O_7 formation in detail. They measured the rate of weight gain for UO_2 powders and wafers excised from unirradiated UO_2 fuel pellets. They reported that parabolic kinetics were observed in the early stages (up to 1%) of the reaction for the sintered pellets. Most of the data reported by Blackburn et al. [4] were measured in oxygen at a pressure of 0.1 atm (10 kPa); however, they did not find a dramatic effect on oxidation rate between 0.1 and 1.0 atm of O_2.

Blackburn et al. [4] fitted their kinetic data to Eq. (6). The resulting values of k have been converted to SI units and summarized in Table 1. Note that where more than one value of k was reported for a given temperature, the average value is listed in Table 1.

Table 2
Empirically determined rate constants κ (s^{-1}) and k ($m^2\ s^{-1}$) calculated from kinetic data reported by Aronson et al. (1957)

Temp. (°C)	Particle size (m)	κ (s^{-1})	k ($m^2\ s^{-1}$)
161	1.3×10^{-7}	5.16×10^{-6}	8.55×10^{-20}
182	5×10^{-7}	1.16×10^{-6}	2.84×10^{-19}
183	5×10^{-7}	1.75×10^{-6}	4.29×10^{-19}
198	5×10^{-7}	3.02×10^{-6}	7.40×10^{-19}
200	5×10^{-7}	2.83×10^{-6}	6.94×10^{-19}
201	1.3×10^{-7}	4.46×10^{-5}	7.39×10^{-19}
217	5×10^{-7}	8.10×10^{-6}	1.98×10^{-18}
230	5×10^{-7}	1.26×10^{-5}	3.08×10^{-18}
230	1.3×10^{-7}	2.30×10^{-4}	3.81×10^{-18}
234	5×10^{-7}	1.31×10^{-5}	3.21×10^{-18}
235	5×10^{-7}	1.20×10^{-5}	2.94×10^{-18}
236	5×10^{-7}	1.14×10^{-5}	2.79×10^{-18}
238	5×10^{-7}	1.60×10^{-5}	3.92×10^{-18}
258	5×10^{-7}	2.23×10^{-5}	5.46×10^{-18}
260	5×10^{-7}	3.28×10^{-5}	8.04×10^{-18}
273	5×10^{-7}	7.25×10^{-5}	1.78×10^{-17}
275	5×10^{-7}	1.00×10^{-4}	2.45×10^{-17}
276	5×10^{-7}	6.09×10^{-5}	1.49×10^{-17}
276	5×10^{-7}	1.06×10^{-4}	2.60×10^{-17}
277	5×10^{-7}	7.77×10^{-5}	1.90×10^{-17}
278	5×10^{-7}	8.35×10^{-5}	2.05×10^{-17}
299	5×10^{-7}	2.84×10^{-4}	6.96×10^{-17}
300	5×10^{-7}	2.90×10^{-4}	7.11×10^{-17}
304	5×10^{-7}	3.25×10^{-4}	7.96×10^{-17}
321	5×10^{-7}	5.40×10^{-4}	1.32×10^{-16}
325	5×10^{-7}	1.28×10^{-3}	3.14×10^{-16}
348	5×10^{-7}	1.45×10^{-3}	3.55×10^{-16}
350	5×10^{-7}	3.25×10^{-3}	7.96×10^{-16}

3.1.4. The data of Walker

Walker [41] gravimetrically measured the rate of oxidation in air of both powders and pellets of unirradiated UO_2. He reported that the kinetic data could be fitted to either Eq. (3) or Eq. (6). Values of the rate constant k were not reported for individual temperatures; rather, values of the pre-exponential factor, k_o, and the activation energy, E_a, were given for the Arrhenius expression

$$k = k_o e^{-\frac{E_a}{RT}} \tag{12}$$

To compare Walker's kinetic data with the others discussed herein, the value of k was calculated from Eq. (12) for the finely divided ($r = 1.0 \times 10^{-7}$ m) UO_2 powder described in his Fig. 1, for each temperature shown therein. Calculated values of the oxidation rate constant k, based on the data of Walker, are presented in Table 1.

3.1.5. The data of Woodley et al.

Woodley et al. [37,38] oxidized fragments of used LWR fuel in air in the range 140 to 225°C and measured

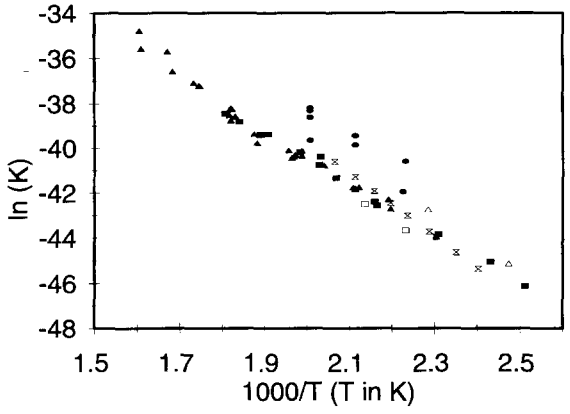

Fig. 1. Arrhenius plot for the diffusion-controlled parabolic rate constant for the formation of U_4O_9/U_3O_7 on UO_2. References for the various data are: (■) [4], (□) [18], (●) [37,38], (⋈) [41], (▲) [1], (△) [5].

the extent of oxidation by weight gain. They reported that oxidation proceeds by migration along the grain boundaries and then by intragranular progression of a layer of U_4O_9. The kinetic data were thus fitted to Eq. (10) and the calculated values of κ were converted to the corresponding values of k by use of Eq. (11). Since the used fuel was found to oxidize by oxygen transport along the grain boundaries with subsequent diffusion through a U_4O_9 layer into each individual grain [37,38], the effective particle size, r, used in Eq. (11) was the grain size of the initial UO_2. The majority of the oxidation tests were performed on used LWR fuel from Fuel Rod G7 from the 15×15 Turkey Point Fuel Assembly B17. The mean number of grain boundary intercepts in Fuel Rod G7 was found to be 53.8 per mm [42], which corresponds to a mean grain diameter of 0.0186 mm. For comparison with the results of other investigators, we thus assume herein that the grains in Fuel Rod G7 are spherical with radius 9.3×10^{-6} m, which is significantly larger than the grain size of typical LWR fuel.

Woodley et al. [38] found that the experimentally determined values of κ are a function of the degree of oxidation and that a true steady state value of k is only obtained at $\Delta(O/M)$ values of ~ 0.1 or greater. We therefore use the values of κ corresponding to $\Delta(O/M) = 0.11$ reported by Woodley et al. [37] for calculation of the diffusion-controlled rate constant, k. The values of k were calculated using Eq. (11) with values of $r = 9.3 \times 10^{-6}$ m and $a = 0.99$. The results of such calculations are presented in Table 1.

3.1.6. The data of Einziger et al.

Einziger et al. [18] studied the rate of U_4O_9 formation by using an SEM imaging technique to measure directly the rate of intragranular growth of the oxide layer. Used fuel fragments and coarse powders from LWR reactors were oxidized at 175 and 195°C in air. The samples did not display completely uniform oxidation; however, the authors were able to study the oxidation kinetics in those regions of the samples that displayed uniform rates of intragranular oxidation. The kinetic data suggested that U_4O_9 formation obeys parabolic kinetics. The rate constant k (Eq. (6)) was found to be 1.11×10^{-19} and 3.50×10^{-19} $m^2\ s^{-1}$ at 175 and 195°C, respectively.

3.1.7. Summary of diffusion-controlled kinetic data

Values of the parabolic rate constant, k, calculated from the kinetic data presented by various investigators [1,4,5,18,37,38,41] are displayed as an Arrhenius plot in Fig. 1.

The agreement between rate constants calculated from the results of various investigators is generally good, considering the various types of fuel oxidized and the variety of experimental techniques employed. The gravimetric data reported by Woodley et al. [37,38] display significantly higher rate constants than the other results. It is not clear if the differences are due to the assumption used herein of spherical grains in the spent LWR fuel, or because of radiation-enhanced oxygen diffusion rates in used fuel. Differences between the gravimetric kinetic data of Woodley et al. [37,38] and the SEM data reported by Einziger et al. [18] are interesting; the differences may be due to the spherical-grain assumption used herein, or may be simply due to sample-to-sample variations in oxidation behaviour for used LWR fuel, which can be substantial [18,43]. Because of uncertainties in the oxidation behaviour of used fuel, the data of Woodley et al. [37,38] and Einziger et al. [18] were not used in the determination of the activation energy for the diffusion-controlled formation of U_3O_7 on UO_2.

The spent LWR fuel data were removed from Fig. 1 and a linear regression was performed on the remaining

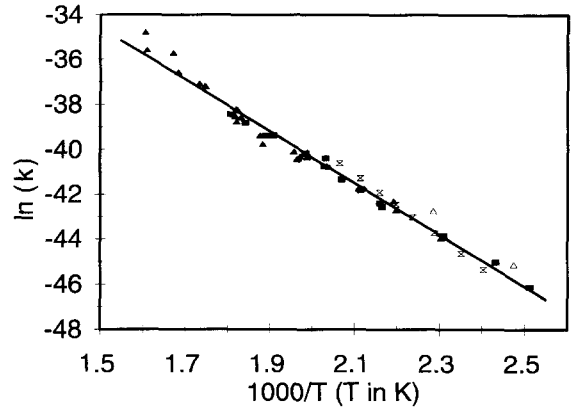

Fig. 2. Arrhenius plot for the diffusion-controlled parabolic rate constant for the formation of U_4O_9/U_3O_7 on UO_2. Data for the oxidation of used LWR fuel [37,38,18] are not included. References for the various data are: (■) [4], (⋈) [41], (▲) [1], (△) [5].

Table 3
Published estimates of the activation energy for the formation of U_4O_9/U_3O_7 on unirradiated UO_2 and spent LWR fuel

Investigator	Material	Temp. range (°C)	E_{act} (kJ mol^{-1})
Anderson et al. (1955)	UO_2 powder	131–164.5	104 [a]
Aronson et al. (1957)	UO_2 powder	161–350	102 [a]
Blackburn et al. (1958)	UO_2 pellets and powder	125–280	90.8
Walker (1965)	UO_2 powder	143–211	120 ± 8
Einziger et al. (1992)	spent LWR fuel	175–195	100
Woodley et al. (1988, 1989)	spent LWR fuel	175–225	113 ± 17

[a] Activation energy re-calculated from investigators original data using the discrete-layer kinetic model (rather than the concentration-gradient model).

data. The resulting Arrhenius plot is shown in Fig. 2. The linear regression gave the following Arrhenius relation for the parabolic rate constant:

$$\ln(k) = -\frac{95.7\ \text{kJ mol}^{-1}}{R} \cdot \frac{1}{T} - 17.33. \quad (13)$$

The calculated activation energy of 96 kJ mol^{-1} is lower than most of the earlier published values summarized in Table 3. However, the consistency between the activation energy calculated herein and the data published earlier (Table 3) is reasonably good considering the range of sample types and experimental techniques used in the earlier studies.

3.2. Linear kinetic data

Several investigators have reported that the rate of U_3O_7 formation displays linear kinetic behaviour. As noted below, most of these data apply to unirradiated sintered UO_2 pellets. Linear rate constants from the following four studies are compiled in Table 4.

3.2.1. The data of Smith

Smith [44] studied the rate of oxidation of unirradiated UO_2 pellets by measuring the pressure decrease associated with the reaction. He reported that the quantity of U_3O_7 increases linearly with time and interpreted this to mean that the reaction was diffusion controlled through a constant-thickness product layer (i.e., that oxygen diffusion through UO_2 is faster than through U_3O_7). Kinetic data measured by Smith were for 600 Torr of O_2, but are likely applicable to air oxidation, since the rate of oxidation is almost independent of oxygen partial pressure above ~ 150 Torr [4].

3.2.2. The data of Taylor et al.

Taylor et al. [32] measured the rate of formation of U_3O_7 on the surface of polished disks, cut from unirradiated CANDU fuel pellets, by quantitative analysis of the X-ray diffraction (XRD) patterns. Samples oxidized in laboratory air in the range 216 to 275°C displayed linear rates of U_3O_7 growth in the early stages of the reaction.

3.2.3. The data of Tempest et al.

Tempest et al. [33] measured the rate of U_3O_7 formation on the surface of planchets excised from unirradiated advanced gas-cooled reactor (AGR) fuel pellets and subsequently oxidized in air at 230°C. Quantitative analysis of

Table 4
Linear rate constant (k') for the first stage of UO_2 oxidation

Investigator	Sample	Method	Temp. (°C)	k' (m s^{-1})
Taylor et al. (1980)	sintered UO_2 pellets	XRD	216	2.5×10^{-12}
			229	3.6×10^{-12}
			238	6.4×10^{-12}
			250	1.3×10^{-11}
			264	2.86×10^{-11}
			275	3.89×10^{-11}
Tempest et al. (1988)	sintered UO_2 pellets	XRD	230	1.42×10^{-12}
Smith (1960)	sintered UO_2 pellets	ΔP	225	6.1×10^{-12}
			250	8.6×10^{-12}
			275	3.97×10^{-11}
Thomas and Einziger (1992)	used LWR fuel	SEM	195	1.31×10^{-12}

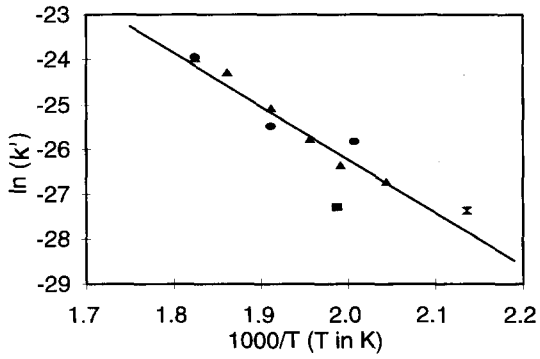

Fig. 3. Arrhenius plot for the linear rate constant (k') for the formation of U_4O_9/U_3O_7 on UO_2. References for the various data are: (■) [33], (●) [44], (▲) [32], (⋈) [9].

the XRD patterns showed that the thickness of the U_3O_7 layer increases linearly with time at a rate of 1.42×10^{-12} m s^{-1}.

3.2.4. The data of Thomas and Einziger

Thomas and Einziger [9] studied the formation of U_4O_9 on used LWR fuel by the anomalous electron backscattering SEM technique. They reported that at 195°C the thickness of the U_4O_9 layer increases linearly with time in the early stages of the reaction, that is, for samples oxidized to compositions between $UO_{2.04}$ and $UO_{2.16}$. The reported value for the rate of intragranular oxidation was 4.7 nm $h^{-1} = 1.31 \times 10^{-12}$ m s^{-1}.

3.2.5. Summary of the linear kinetic data

Linear kinetic behaviour in the first stage of the oxidation of sintered UO_2 pellets is clearly an approximation of a multifarious process involving cracking and both grain-boundary and intragranular oxidation. There is thus no obvious reason to expect Arrhenius behaviour to be observed for the linear kinetic data. Nonetheless, an Arrhenius plot (Fig. 3) displays reasonably good linear behaviour. Linear regression of the data displayed in Fig. 3 gives the expression

$$\ln(k') = -\frac{98.6 \text{ kJ mol}^{-1}}{R} \cdot \frac{1}{T} - 2.513. \quad (14)$$

The calculated activation energy of 98.6 kJ mol^{-1} is very similar to the value of 95.7 kJ mol^{-1} derived from diffusion-controlled kinetic data in Section 3.1.7. The similarity between the two activation energies may suggest that the rate of oxygen diffusion dominates the kinetic expression for the rate of oxidation of sintered UO_2 pellets.

4. Implications for the dry air storage of used CANDU fuel

Oxidation of unirradiated CANDU fuel pellets starts with the formation of a homogeneous layer of U_3O_7 on the sample surface and then proceeds inward along an oxidation front, which becomes more convoluted with the evolution of time [32]. In contrast, oxidation of used LWR fuel to U_4O_9 proceeds in most cases by rapid grain-boundary oxidation, followed by intragranular oxidation as a discrete layer around each UO_2 grain [9,18]. However, some samples of used LWR fuel display regions of inhomogeneous oxidation and the existence of oxidation fronts [40].

Experimental evidence suggests that the low-temperature oxidation behaviour of used CANDU fuel is intermediate between that of unirradiated UO_2 and that of used LWR fuel. Oxidation of used CANDU fuel in dry air generally advances rapidly (relative to unirradiated UO_2) via cracks and grain boundaries, so that intragranular oxidation occurs simultaneously over large portions of the sample as shown in Fig. 4. For example, oxidation in limited dry air (150°C) of deliberately defected used CANDU fuel elements displayed a higher degree of oxidation in the vicinity of the defect, but significant oxidation to U_3O_7 was widespread throughout the sample [6]. Similarly, recent experiments in which these deliberately defected CANDU fuel elements were further oxidized in unlimited dry air (150°C, 40 months) displayed essentially complete oxidation to U_3O_7 throughout the sample, but minimal conversion to U_3O_8 [45].

Experimental evidence suggests [6,45] that near 150°C oxygenic diffusion along the grain boundaries of used CANDU fuel is rapid relative to that of unirradiated UO_2. Therefore, oxidation of used CANDU fuel near such temperatures can be considered, to a first approximation, as equivalent to oxidation of a UO_2 powder, with particle size equal to the grain size of the used fuel. The impact of U_3O_7 formation on weight-gain experiments will thus likely be significant. Consider, for example, the weight-gain experiments of Hastings et al. [46,47]. They oxidized

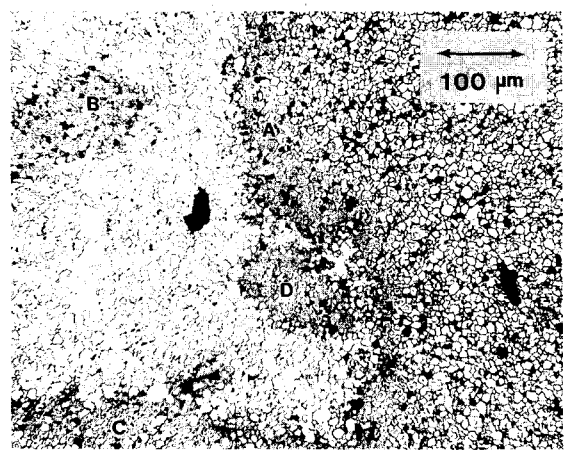

Fig. 4. Optical micrograph (200×) of etched used CANDU fuel after oxidation at 150°C for ~ 100 months in limited dry air and a further 40 months in unlimited dry air. An oxidation front is present (A) while several other regions (B, C, D) are also undergoing simultaneous oxidation. Photo courtesy of Ken Wasywich.

fragments of both unirradiated and irradiated CANDU fuel in the range 175 to 400°C. They reported that the rate of weight gain for irradiated CANDU fuel fragments is given by

$$F = 1.53 \times 10^{10}\, e^{(-(120 \pm 10\ \text{kJ mol}^{-1}/RT))}, \quad (15)$$

where F is the rate of weight gain in % per h. The analogous expression for the rate of weight gain for unirradiated UO_2 fragments was

$$F = 1 \times 10^{12}\, e^{(-(140 \pm 10\ \text{kJ mol}^{-1}/RT))}. \quad (16)$$

Fragment size was uniform at ~ 1 g [47] and the grain size was 1×10^{-5} m diameter [46]. The theoretical density of UO_2 is 1.096×10^7 g m^{-3}, thus the volume of a single fragment was 9.124×10^{-8} m^3. At low (< 200°C) temperatures, the oxidation behaviour of a 1 g fragment is considered equivalent to the same mass of powder, which would consist of 1.80×10^8 particles of radius 5×10^{-6} m and would have a surface area of 5.65×10^{-2} m^2 g^{-1}. The initial rate of oxidation can be considered by estimating the time required for the formation of a 1 μm thick layer on the surface of each particle. The fraction of the total sample oxidized at this time would be 0.488.

The rate constant (k) for the parabolic kinetic model is estimated from Eq. (13) to be 2.09×10^{-19} m^2 s^{-1} at 175°C. According to Eq. (6) a 1 μm thick layer of U_3O_7 will form in 4.79×10^6 s, which corresponds to an average oxidation rate of 7.2×10^{-4}% h^{-1}. Similarly, the linear rate constant (k') for U_3O_7 formation can be estimated from Eq. (14) to be 2.61×10^{-13} m s^{-1} at 175°C. The time required for the formation of a 1 μm thick layer of oxide can thus be calculated as 3.84×10^6 s. The corresponding rate of oxidation is 9.01×10^{-4}% h^{-1}.

The initial rate of oxidation predicted by both the linear and parabolic models is greater than the rate of weight gain (1.58×10^{-4}% h^{-1}) calculated for used CANDU fuel at 175°C using Eq. (15). The fact that calculated estimates of the rate of weight gain are higher than experimentally observed [47] is not particularly important, since it is probably associated with non-uniform oxidation resulting from slow grain-boundary oxidation in some regions of the samples [6] (recall that dry air oxidation of used CANDU fuel is generally not as uniform as is the case with used LWR fuel). The important point is that the predicted rate of U_3O_7 formation is ample to account for all of the observed weight gain at 175°C in the experiments of Hastings et al. [46,47]. Thus it seems probable that the weight gain observed in dry air oxidation of used CANDU fuel [46,47] was mostly associated with the formation of U_3O_7 at low (< 200°C) temperatures.

Above 300°C the weight gain data reported by Hastings et al. [46,47] would be associated primarily with U_3O_8 formation [4], so the results reported by Hastings et al. [46,47] for irradiated CANDU fuel likely represent the aggregate of weight gains associated with both U_3O_7 and U_3O_8 formation. Thus it is not surprising that the reported activation energy for the formation of 'U_3O_8' in irradiated CANDU fuel [47] is 120 kJ mol^{-1}, which is approximately equal to the average of the value (140 kJ mol^{-1}) reported for U_3O_8 formation on unirradiated fuel [47] and the value (96 kJ mol^{-1}) shown (Eq. (13)) to be valid for the intragranular rate of formation of U_3O_7.

The analysis presented herein suggests that the reported activation energy (120 kJ mol^{-1}) for the formation of 'U_3O_8' on used CANDU fuel [46,47] is probably too low. When the reported oxidation rates are extrapolated to lower temperatures, they lead to unduly conservative estimates of the rate of U_3O_8 formation during the dry air storage of used CANDU fuel. A more accurate method for the study of U_3O_8-formation kinetics has recently been developed [48] by use of XRD to measure specifically the rate of formation of U_3O_8 on the surface of UO_2 samples. Such a technique can provide the best information of the allowable upper limit for the dry air storage of used CANDU fuel.

5. Conclusions

Kinetic data on the rate of U_4O_9/U_3O_7 formation on UO_2 have been critically reviewed. Oxidation of unirradiated UO_2 powders results in the formation of U_3O_7 by parabolic kinetics because the limiting step of the reaction is diffusion through a discrete layer of the product oxide. Used LWR fuel samples have rapid grain-boundary oxidation, so that oxidation proceeds in such samples much like oxidation of a powder sample having particle size equal to the grain size of the used fuel. In contrast, unirradiated, sintered UO_2 pellets display linear oxidation kinetics, presumably because the rate of oxidation is controlled by a combination of grain-boundary oxidation, cracking and intragranular oxidation.

Critical review of the literature yields consistent estimates of the activation energy for the formation of U_3O_7 on UO_2 powders (96 kJ mol^{-1}) and unirradiated, sintered UO_2 pellets (99 kJ mol^{-1}).

Analysis of the rate of U_3O_7 formation on irradiated CANDU fuel fragments indicates that weight-gain experiments [46,47] may have underestimated the activation energy for the formation of U_3O_8 on used CANDU fuel.

Acknowledgements

The author appreciates critical review of this manuscript by Peter Taylor and Ken Wasywich.

References

[1] S. Aronson, R.B. Roof Jr. and J. Belle, J. Chem. Phys. 27 (1957) 137.

[2] M.J. Bannister, J. Nucl. Mater. 26 (1968) 174.
[3] H.R. Hoekstra, A. Santoro and S. Siegel, J. Inorg. Nucl. Chem. 18 (1961) 166.
[4] P.E. Blackburn, J. Weissbart and E.A. Gulbransen, J. Phys. Chem. 62 (1958) 902.
[5] J.S. Anderson, L.E.J. Roberts and E.A. Harper, J. Chem. Soc. (1955) 3946.
[6] K.M. Wasywich, W.H. Hocking, D.W. Shoesmith and P. Taylor, Nucl. Technol. 104 (1993) 309.
[7] K.J. Schneider, S.J. Mitchell and A.B. Johnson Jr., Proc. 3rd Int. Conf. High Level Radioactive Waste Management, Las Vegas, NV, USA, Apr. 12–16, 1992 (American Nuclear Society, La Grange Park, IL, 1992).
[8] D.G. Boase and T.T. Vandergraaf, Nucl. Technol. 32 (1977) 60.
[9] L.E. Thomas and R.E. Einziger, Mater. Charact. 28 (1992) 149.
[10] R.E. Einziger and R.E. Woodley, Proc. Workshop on Chemical Reactivity of Oxide Fuel and Fission Product Release, Berkeley, UK, Apr. 7–9, 1987 (Central Electricity Generating Board, UK, 1987).
[11] R.E. Einziger and J.A. Cook, Nucl. Technol. 69 (1985) 55.
[12] J. Novak, I.J. Hastings, E. Mizzan and R.J. Chenier, Nucl. Technol. 63 (1983) 254.
[13] M. Guyonvarh and R. Le Meur, Evolution D'Echantillons De Bioxyde D'Uranium Apres Rupture De Gaine, Report CEA-R 3329 (1967).
[14] L.E. Thomas, R.E. Einziger and H.C. Buchanan, J. Nucl. Mater. 201 (1993) 310.
[15] N. Masaki, J. Nucl. Mater. 101 (1981) 229.
[16] D.J.M. Bevan, I.E. Grey and B.T.M. Willis, J. Solid State Chem. 61 (1986) 1.
[17] B.T.M. Willis, J. Chem. Soc., Faraday Trans. II 83 (1987) 1073.
[18] R.E. Einziger, L.E. Thomas, H.C. Buchanan and R.B. Stout, J. Nucl. Mater. 190 (1992) 53.
[19] H.R. Hoekstra, S. Siegel and F.X. Gallagher, J. Inorg. Nucl. Chem. 32 (1970) 3237.
[20] D.K. Smith, B.E. Scheetz, C.A.F. Anderson and K.L. Smith, Uranium 1 (1982) 79.
[21] P. Pério, doctoral dissertation, University of Paris (1955); CEA (France), Report No. 363.
[22] K.B. Alberman and J.S. Anderson, J. Chem. Soc. (1949) S303.
[23] Y. Saito, Nihon Kinzoku Gakkai-shi 39 (1975) 760.
[24] H. Ohashi, E. Noda and T. Morozumi, J. Nucl. Sci. Technol. 11 (1974) 445.
[25] J. Crank, The Mathematics of Diffusion (Clarendon, Oxford, 1956).
[26] G. Jander, Z. Anorg. Chem. 163 (1927) 7.
[27] G. Valensi, C. R. 202 (1936) 309.
[28] C. Wagner and K. Grunewald, Z. Phys. Chem. B40 (1938) 455.
[29] J.S. Anderson, Bull. Soc. Chim. Fr. 20 (1953) 781.
[30] S. Whillock and J.H. Pearce, J. Nucl. Mater. 175 (1990) 121.
[31] B.E. Schaner, J. Nucl. Mater. 2 (1960) 110.
[32] P. Taylor, E.A. Burgess and D.G. Owen, J. Nucl. Mater. 88 (1980) 153.
[33] P.A. Tempest, P.M. Tucker and J.W. Tyler, J. Nucl. Mater. 151 (1988) 251.
[34] J.B. Price, M.J. Bennett, F.L. Cullen, J.F. Norton and S.R. Canetoli, Proc. 1st Int. Conf. Microscopy of Oxidation, Cambridge, UK (1991).
[35] L.E. Thomas, R.E. Einziger and R.E. Woodley, J. Nucl. Mater. 166 (1989) 243.
[36] P. Taylor, D.D. Wood, D.G. Owen, W.G. Hutchings, A.M. Duclos, Microstructures and Phase Relationships of Crystalline Oxidation Products Formed on Unused CANDU Fuel Exposed to Aerated Steam and Aerated Water Near 200°C, Atomic Energy of Canada Limited Report AECL-10476 (1991).
[37] R.E. Woodley, R.E. Einziger and H.C. Buchanan, Measurement of the Oxidation of Spent Fuel Between 140° and 225°C by Thermogravimetric Analysis, Westinghouse Hanford Company, Report WHC-EP-0107 (1988).
[38] R.E. Woodley, R.E. Einziger and H.C. Buchanan, Nucl. Technol. 85 (1989) 74.
[39] J. Nakamura, T. Otomo, T. Kikuchi and S. Kawasaki, J. Nucl. Sci. Technol. 32 (1995) 57.
[40] L.E. Thomas, O.D. Slagle and R.E. Einziger, J. Nucl. Mater. 184 (1991) 117.
[41] D.E.Y. Walker, J. Appl. Chem. 15 (1965) 128.
[42] R.B. Davis and V. Pasupathi, Data Summary Report for the Destructive Examination of Rods G7, G9, J8, I9 and H6 from Turkey Point Fuel Assembly B17, Hanford Engineering Development Laboratory, Report HEDL-TME 80-85 (1981).
[43] R.E. Einziger, S.C. Marschman and H.C. Buchanan, Nucl. Technol. 94 (1991) 383.
[44] T. Smith, Kinetics and Mechanism of the Oxidation of Uranium Dioxide and Uranium Dioxide Plus Fissia Sintered Pellets, Atomics International Report NAA-SR-4677 (1960).
[45] K. Wasywich, AECL Research (1995), personal communication.
[46] I.J. Hastings, E. Mizzan, A.M. Ross, J.R. Kelm, R.J. Chenier, D.H. Rose and J. Novak, Nucl. Technol. 68 (1985) 40.
[47] I.J. Hastings, D.H. Rose, J.R. Kelm, D.A. Irvine and J. Novak, J. Am. Ceram. Soc. 69 (1986) C-16.
[48] R.J. McEachern, J.W. Choi, M. Kolar, W. Long, P. Taylor and D.D. Wood, to be published.